buildings

MDPI

Article

Experimental Study on Characteristics of Pile-Soil Interaction in Screw Piles

Jiakuan Ma [1], Lijuan Luo [1,2,*], Tong Mu [1], Hongtao Guo [1,3] and Yong Tang [1]

[1] School of Civil Engineering, Chang'an University, Xi'an 710061, China
[2] Institute of Underground Structure and Engineering, Chang'an University, Xi'an 710061, China
[3] The 6th Engineering Co., Ltd. of CTCE Group, Xi'an 710002, China
* Correspondence: luojuan@chd.edu.cn; Tel.: +86-02982337356

Abstract: A screw pile is a special-shaped pile with several advantages, including good bearing capacity, economy, and rapid construction. The calculation of the screw piles' ultimate bearing capacity in the individual bearing failure state remains controversial. To address the problems of an unclear failure mechanism and the pile–soil contact relationship in screw piles, we conducted large-scale direct shear tests using a partial amplification method. The variation law for soil stress and the failure pattern of soil around the screw teeth were analyzed. The bearing capacity of the screw shear plate with screw teeth was found to be significantly higher than that of the plane shear plate, while that of the screw pile first increased and then decreased with an increase in the screw pitch. The optimal screw pitch allowed the determination of the maximum bearing capacity. Furthermore, the optimal screw pitch was generally equal to the critical screw pitch, which distinguished the individual bearing failure from the cylindrical shearing failure. A new calculation method for the critical screw pitch and ultimate bearing capacity in the individual bearing failure state was presented, and its rationality was proved using the direct shear test results. The calculation of the critical screw pitch considers the shear strength of soil and the geometric parameters of the screw teeth, making it more widely applicable. These results can provide a theoretical basis for the subsequent design of screw piles.

Keywords: screw pile; large-scale direct shear test; pile-soil contact relationship; critical screw pitch; individual bearing failure

Citation: Ma, J.; Luo, L.; Mu, T.; Guo, H.; Tang, Y. Experimental Study on Characteristics of Pile-Soil Interaction in Screw Piles. *Buildings* **2022**, *12*, 2091. https://doi.org/10.3390/buildings12122091

Academic Editor: Eden Bojórquez

Received: 17 October 2022
Accepted: 15 November 2022
Published: 29 November 2022

1. Introduction

With the continuous development of pile foundations, various special-shaped piles have emerged. Representative examples include the x-shaped pile, the y-shaped pile, the squeezed branch pile, and the screw pile [1–6]. Among these special-shaped piles, screw piles have been globally used due to their high bearing capacity, economical rates, high construction speed, and environmental protection capacities [7–9]. Presently, the construction technology for screw piles is relatively mature.

Consistent with differences in structural characteristics, screw piles can be divided into concrete and steel screw piles [10,11] (Figure 1). The steel screw pile was first invented by the British engineer Alexander to strengthen the foundations of lighthouses [12]. It is composed of a steel shaft with several separated helical plates at the bottom of the shaft. In contrast, the screw teeth of the concrete screw piles are spiral and are continuously distributed along the shaft, and the cantilever length of the screw teeth is generally smaller than that of the steel screw piles.

According to existing research, the bearing capacity of the concrete and steel screw piles is significantly higher than that of the round piles under the same conditions [13–15]. Notably, the bearing capacity of the screw piles increases mainly due to screw teeth along the shaft. The screw teeth change the spreading mode of the lateral force around the pile.

The conventional friction contact mode changes into a more complex mode and includes the occlusal effect, the friction effect, and the tip bearing effect. The new mode promotes closer contact between the soil and the pile, distributing the load on the pile more widely across the soil. Consequently, screw piles tend to have a superior bearing capacity.

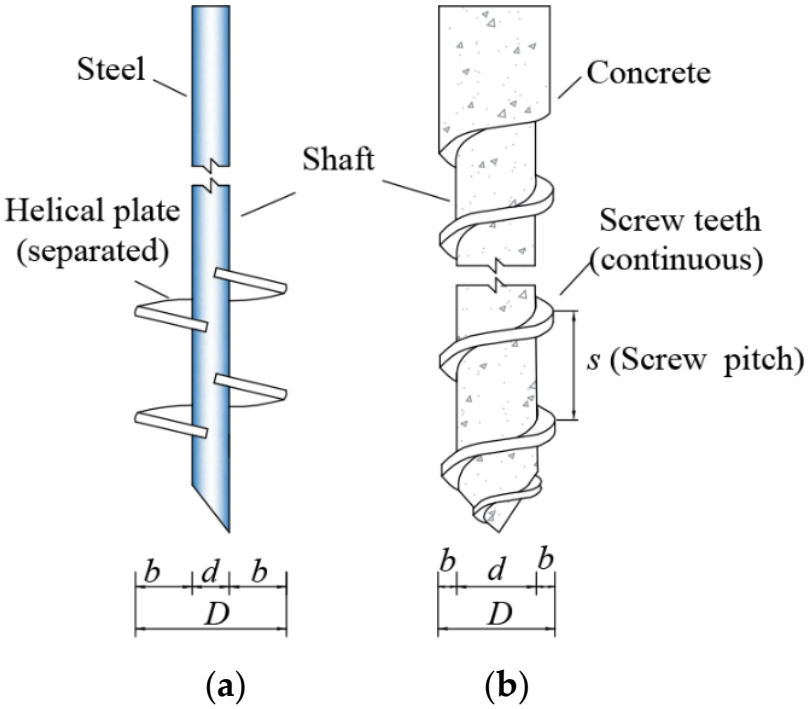

Figure 1. Schematic diagram. (**a**) Steel screw pile and (**b**) concrete screw pile.

Undoubtedly, screw piles have good application prospects in civil construction. Presently, various research results have been published on screw piles, such as those pertaining to the failure mode of the steel screw piles and the influence of the key geometric parameters of screw piles on their bearing capacity [16–19]. The core research problem for screw piles is the contact relationship between the screw teeth and soil. The failure modes of screw piles can be roughly divided into individual bearing failure (IBF) and cylindrical shearing failure (CSF) modes [11,20–22]. When the screw pitch is large, the interaction between the adjacent screw teeth is weak. The force states of each screw tooth level are considered independent, and failures occur separately. The bearing capacity of the pile side is determined by the skin friction of the shaft and the tip resistance of the screw teeth. This failure mode is the IBF mode. When the screw pitch is small, the interaction between adjacent screw teeth is strong, and the failure surface is a round cylindrical surface formed along the periphery of the screw teeth; this is the CSF mode.

For a screw pile in the CSF mode, the method calculating the bearing capacity is similar to that for conventional circular piles. However, for screw piles in the IBF mode, much controversy exists about the failure law of the soil under the screw teeth, and the method for calculating the bearing capacity of the screw teeth is still unclear. Relevant scholars have proposed various failure modes following the bearing theory of strip foundations, such as the Terzaghi, Meyerhof, and cavity expansion failure modes [23–25]; however, determination of the failure type requires further investigation.

To address these issues, large-scale direct shear tests were conducted to investigate the contact relationship between the screw teeth and soil. The optimal screw pitch was obtained by analyzing the variation of the Q–u (load–displacement) curves of the screw shear plates with different screw pitches. Meanwhile, the failure law of the soil around the screw teeth was analyzed by observing the deformation and the stress variation of the soil around the screw teeth of the screw shear plate with the optimal screw pitch. The

theoretical failure model was established, and the calculation equations for the critical screw pitch (s_{cr}) and the bearing capacity were derived.

2. Materials and Methods

2.1. Model Test Object and Similarity Ratio

According to the statistical data provided in the Technical Specifications for Screw Concrete Pile [26], the prototype parameters of the screw piles are selected as follows: the outer diameter D is 500 mm, the inner diameter d is 380 mm, the height of the screw teeth b is 60 mm, the screw pitch s is 540 mm, and the bottom and top thicknesses of the screw teeth are 60 mm and 40 mm, respectively.

The least-explored part of the research on the bearing mechanisms of the screw piles is the contact relationship between the screw teeth and soil, including soil deformation and stress variation. As the pile is a large structure along its length direction, conventional model tests often choose a small geometric scale, most of which are about 1:10. However, using this scale, the height of the screw teeth in this paper is only 6 mm and the screw pitch is 54 mm. The soil deformation and stress monitoring is difficult, which hinders the analyzing their contact relationship. In addition, the pile–soil contact interface of screw piles has complex three-dimensional spiral geometry, so directly studying the interaction law between the screw teeth and soil on a three-dimensional level is difficult [27]. Based on the abovementioned considerations, a partial area was chosen as the test object after unfolding the screw pile (Figure 2).

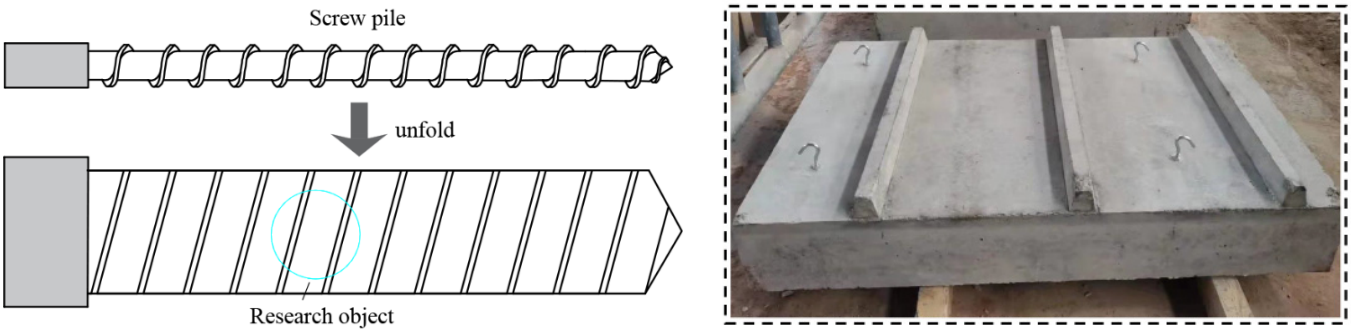

Figure 2. The object of large direct shear test. (**a**) Unfolding diagram and (**b**) screw shear plate.

In order to monitor the soil stress and deformation easily, the geometry scale was set as 1:2. Other physical similarity ratios are listed in Table 1.

Table 1. Similarity ratios of the main physical quantities.

Physical Quantities	Similarity Constant
Geometry	$C_l = 2$
Modulus of elasticity	$C_E = 1$
Strain	$C_\varepsilon = 1$
Stress	$C_\sigma = C_E\, C_\varepsilon = 2$
Poisson ratio	$C_\mu = 1$
Concentrated load	$C_F = C_\sigma\, C_l{}^2 = 4$
Linear load	$C_q = C_\sigma\, C_l = 2$
Area load	$C_p = C_\sigma = 1$

2.2. Test Apparatus and Material

A self-designed large-scale direct shear apparatus was used in the direct shear test, as shown in Figure 3. During the loading process, the upper box is fixed, and the jack pushes the lower box to realize the shearing between the screw shear plates and soil. The size

of the shear plane is 800 mm × 500 mm, and the heights of the upper and lower boxes are 600 mm and 300 mm, respectively. Three indexes were monitored in the direct shear test, including soil deformation, soil stress, and the relative displacement of the upper and lower boxes.

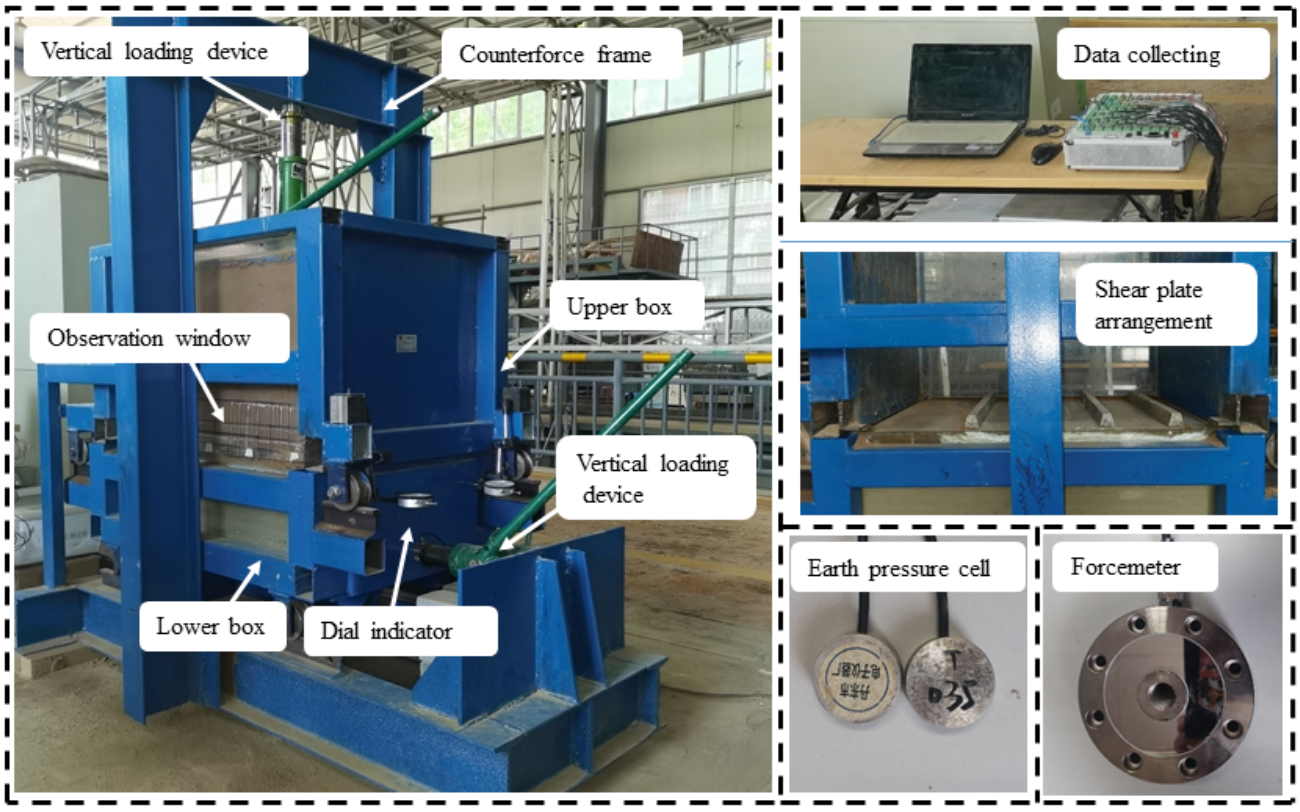

Figure 3. Large-scale direct shear apparatus.

Bx-2 strain-type earth pressure cells were used to monitor the soil stress and have a range of 600 kPa, a precision of 1/1000, and a diameter of 2 cm. The process of burying earth pressure cells is as follows. The compacted thickness of the soil in each layer is 3 cm, which is the same as the height of the screw teeth. After each soil layer is compressed to the designated height, a round hole with a depth of 2 cm and a diameter slightly of more than 2 cm is dug. Subsequently, the earth pressure cell is placed in the designed position. Meanwhile, excavated loose soil is removed, whose weight is equal to the volume of the earth pressure box times the density of compacted soil. Afterward, the remaining soil is evenly buried in the hole and compacted to the design height to ensure that the density of the backfill soil is close to that of the surrounding soil.

Figure 4a shows the front view of the earth pressure cell layout, with three layers in total. Taking Layer 1 as an example, the top view is shown in Figure 4b. Moreover, a deformation monitoring network was formed by burying multiple crossing white lines in the soil near the shear plane, and a line network identical to the monitoring network was drawn on the transparent glass as the reference for the initial position (Figure 4c).

The concrete used in the model piles has a strength grade of C20 ($f_{cu,k}$ = 20 MPa). The mixture ratio was calculated using numerous experiments, and the compressive strength was found to be 21.89 MPa (Table 2). The Young's modulus of concrete was 21.85 GPa. Meanwhile, no reinforcement was installed in the screw teeth for consistency with the practical condition.

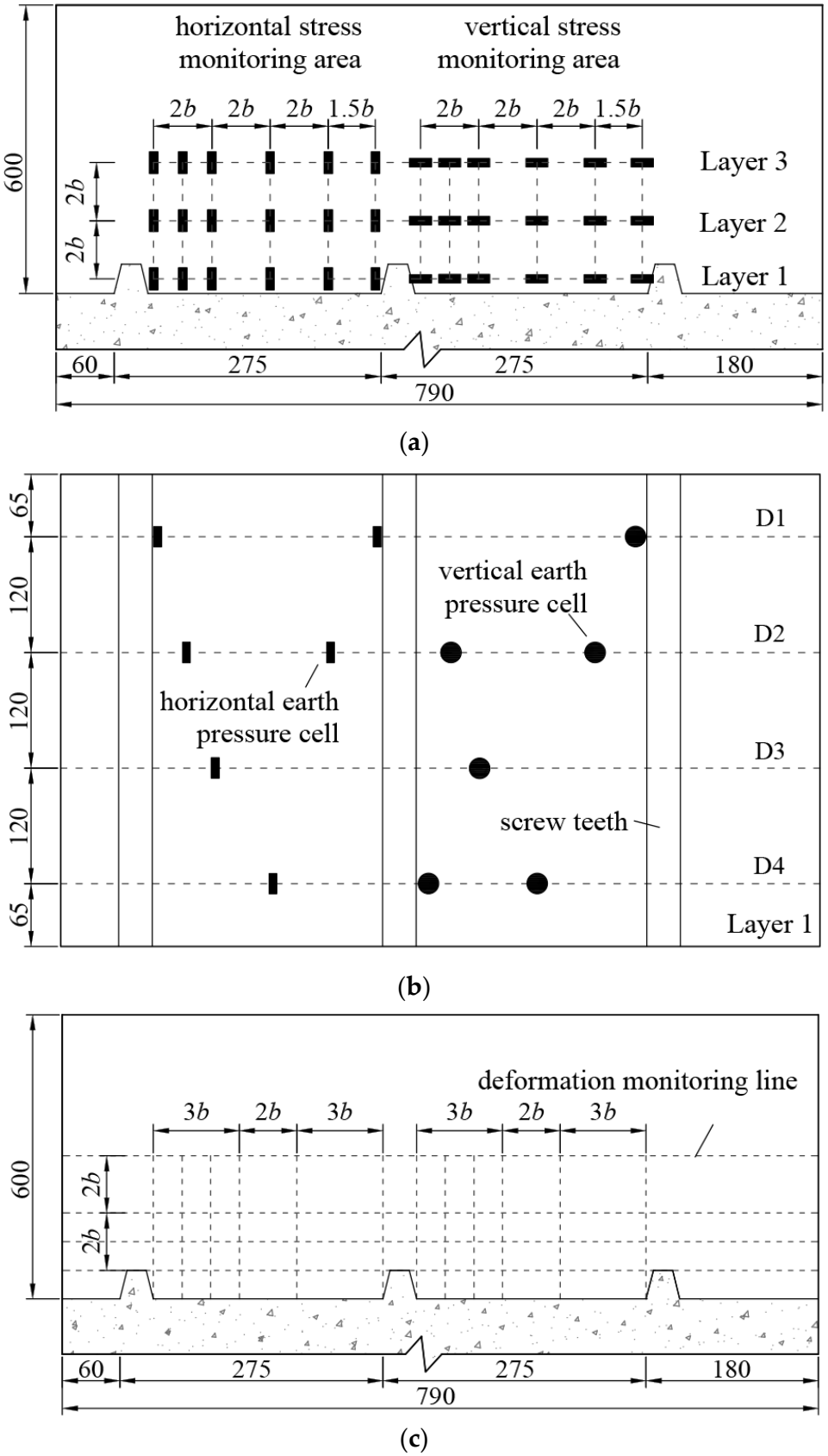

Figure 4. Monitoring arrangement of the 8*b* screw shear plate. (**a**) Front view, (**b**) top view of the earth pressure cell of Layer 1, and (**c**) monitoring network of soil deformation.

Table 2. Mixture ratio of model pile concrete (mass).

Cement	Water	River Sand	Coarse Aggregate
1.00	0.55	1.44	2.08

In addition to the standard screw shear plate (s = 8b), the other three concrete screw shear plates with different screw pitches were prepared for comparative analysis. The screw pitches were 0b (corresponding to the plane shear plate), 4b, and 12b. By analyzing the force laws of the screw shear plates with four screw pitches, the influence of the key parameter, screw pitch s, on the bearing characteristics of the screw piles was obtained. Four different normal pressures of 40 kPa, 80 kPa, 120 kPa, and 160 kPa were applied to each group of tests, corresponding to different burial depths.

Considering the extensive application of screw piles and the prevalence of loess in the western China, the soil used in the direct shear tests was taken from a loess site in Xi'an, a representative city in the loess region. During the test, the soil was re-sieved, filled, and compacted. The changes in the water content and compacting degree were strictly controlled, and the physical indexes of soil in 16 direct shear tests were maintained. The mean value of the physical indexes of soil obtained by laboratory tests is shown in Table 3.

Table 3. Physical indexes of soil (mean).

Index	E_s (MPa)	φ (°)	c (kPa)	ρ (g/cm^3)	w (%)	e
Loess	7.97	28.10	26.80	1.75	14.10	0.76

Concrete screw shear plates with dimensions of 790 mm × 490 mm × 120 mm were placed in the lower box. The height of the screw shear plate was adjusted to be flush with the edge of the lower box by padding a certain thickness of sand and stone mixture. Taking the 8b screw shear plate as an example, the model assembly is shown in Figure 5.

Figure 5. Arrangement of the 8b screw shear plate.

2.3. Loading Procedure

The process of the large-scale direct shear test was as follows: (1) The overlying soil was pre-consolidated under a predetermined normal force using the vertical loading device, and the pre-consolidation time was 24 h. (2) After pre-consolidation, a horizontal load was applied to simulate the vertical force of the screw pile. The step loading method was adopted, and each load level was about 1/10 of the estimated ultimate load. (3) When the displacement rate of the shear plate was less than 0.1 mm/h, it reached a stable state by

default. (4) In the first 15 min of each level of load, the soil stress was first collected at an interval of 20 s and then 60 s. (5) When the *Q*–*u* curve appeared at an obvious inflection point, or the displacement reached 40 mm, the screw shear plates were considered to have reached the ultimate load state.

3. Results

3.1. Macroscopic Shear Characteristics

As shown in Figure 6, the trend of the *Q*–*u* curves of the screw shear plates with 4*b*, 8*b*, and 12*b* screw pitches was the same regardless of their overburden load conditions. There is no sudden surge of displacement during loading, and the overall trend of the gradual change is presented. Although the displacement curves of the plane shear plate (0*b*) showed a sharp decreasing trend, it is mainly caused by the overall coordinate range. When the *Q*–*u* curves of the plane shear plate were drawn separately, the gradual change trend was shown, except for 40 kPa (Figure 7).

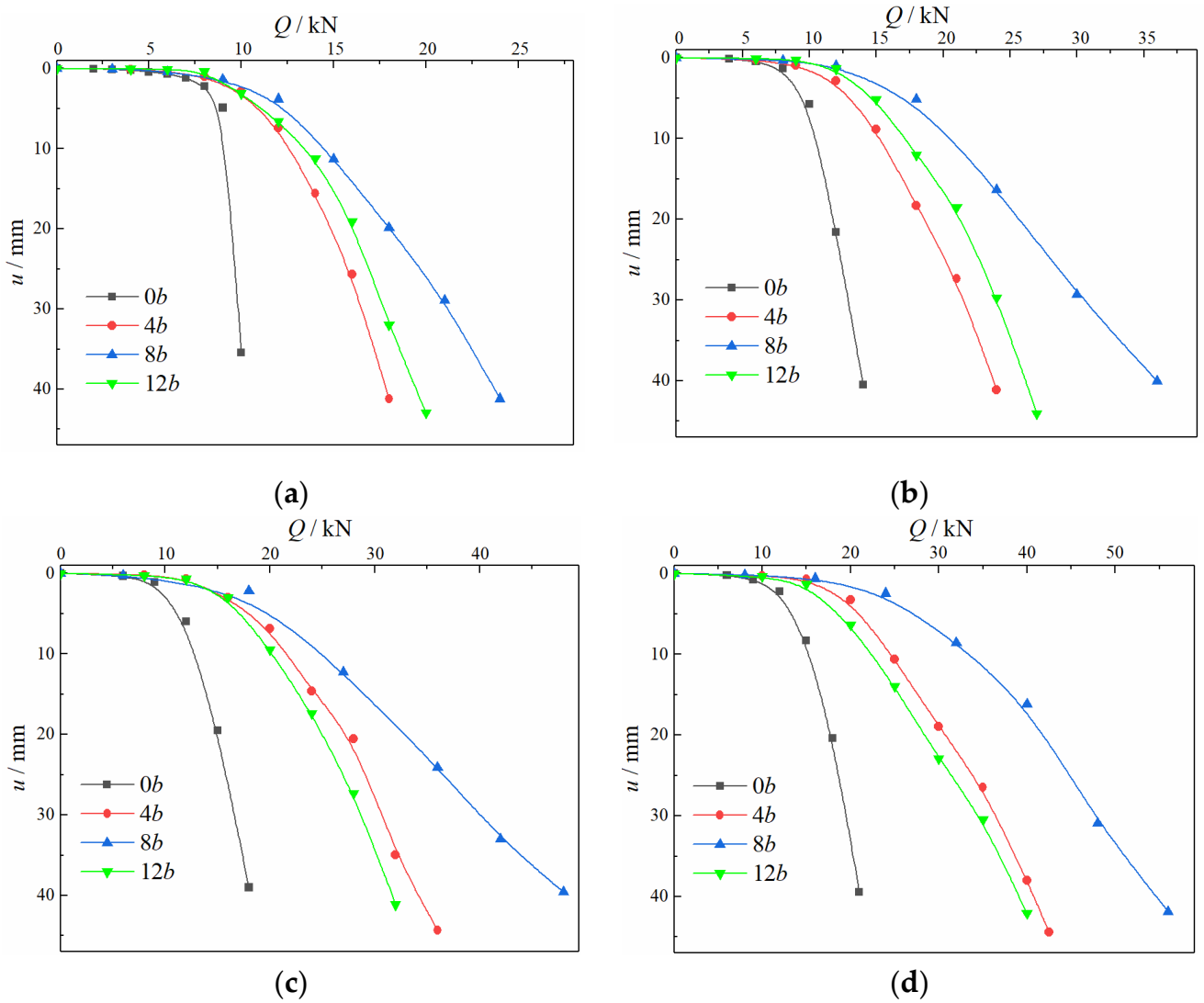

Figure 6. *Q*–*u* curves under different conditions. (**a**) 40 kPa, (**b**) 80 kPa, (**c**) 120 kPa, and (**d**) 160 kPa.

Since each *Q*–*u* curve is under the gradual change trend, the horizontal load when the settlement reaches 40 mm was uniformly selected as the ultimate load according to the Technical Code for Testing of Building Foundation Piles [28]. If there was an obvious inflection point, the corresponding load was chosen as the ultimate bearing capacity.

The Q_{ult} of the plane shear plate under the overburden pressure of 40 kPa to 160 kPa was 9.00 kN, 13.92 kN, 18.07 kN, and 21.08 kN, respectively. In order to further determine the contact relationship between the pile–soil interface, the Q_{ult}–p_0 variation curve of the plane shear plate is drawn (Figure 8), where δ_0 and c_0 are the friction angle and cohesion of the pile–soil interface, respectively, and p_0 is the overburden pressure. The curve presents a linear change trend, and the intercept is not zero. This indicates that, even for conventional circular piles, the interaction between the pile and soil is not only a frictional contact [9,29,30]. However, the interaction may involve more complex contact relationships, including mechanical occlusion, bonding, and chemical cementation, macroscopically shown as c_0. This problem should be considered when analyzing the pile–soil interface interaction to avoid oversimplifying the theoretical model and actual difference.

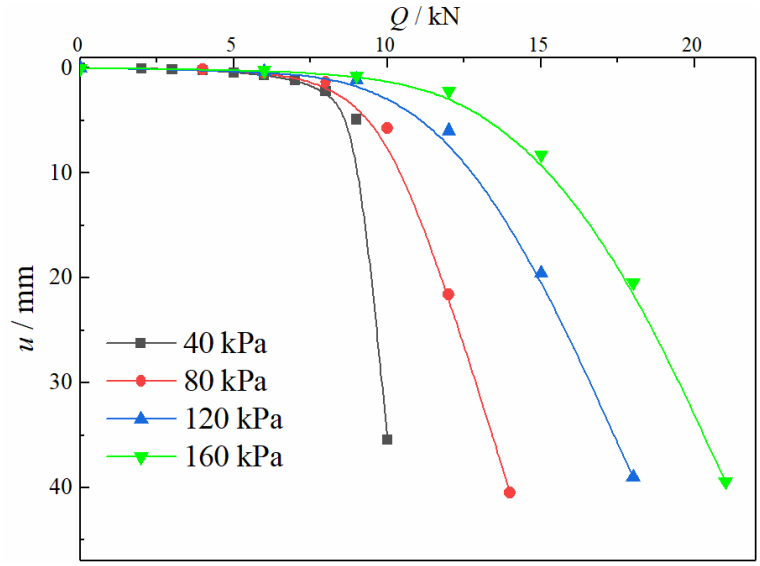

Figure 7. The Q–u curve of the plane shear plate.

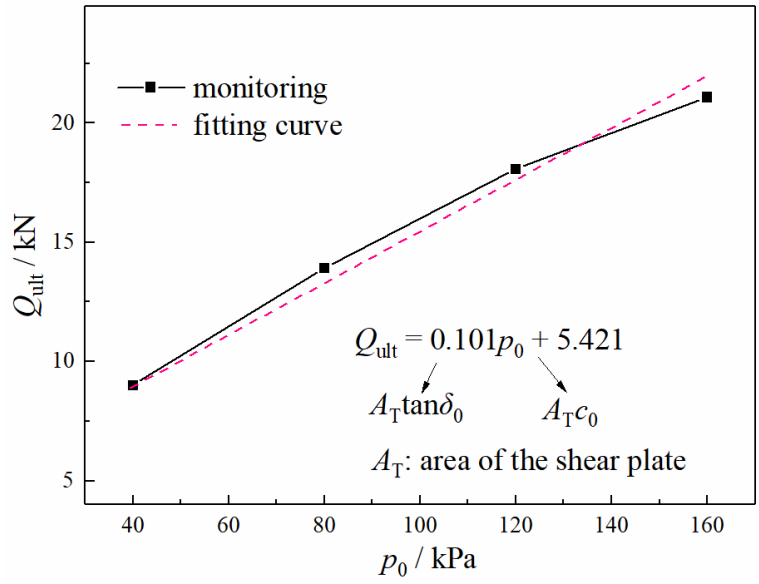

Figure 8. The Q_{ult}–p_0 fitting curve of the plane shear plate.

By analyzing each Q–u curve, it can be found that with an increase in the screw pitch, the bearing capacity of the screw shear plate first increased and then decreased. The bearing capacity of the plane shear plate is the minimum, while the bearing capacities of the 4*b*

and 12*b* screw shear plates are increased and are similar. When the screw pitch was 8*b*, the bearing capacity of the screw shear plate reached its maximum. Compared with other screw shear plates, the *Q*–*u* curves of the 8*b* screw shear plate showed a gradual change trend, indicating that the interaction form is more conducive to load transfer under this condition. The above variation may be due to the bearing effect of the soil around the screw teeth reaching the maximum when the screw pitch reaches a certain value. In this case, the screw pitch is the optimal screw pitch.

In order to analyze the determination method of the optimal screw pitch, the Q_{ult}–*b* curves were drawn and analyzed. The variation curves of the ultimate bearing capacity of the screw shear plates with different screw pitches are shown in Figure 9.

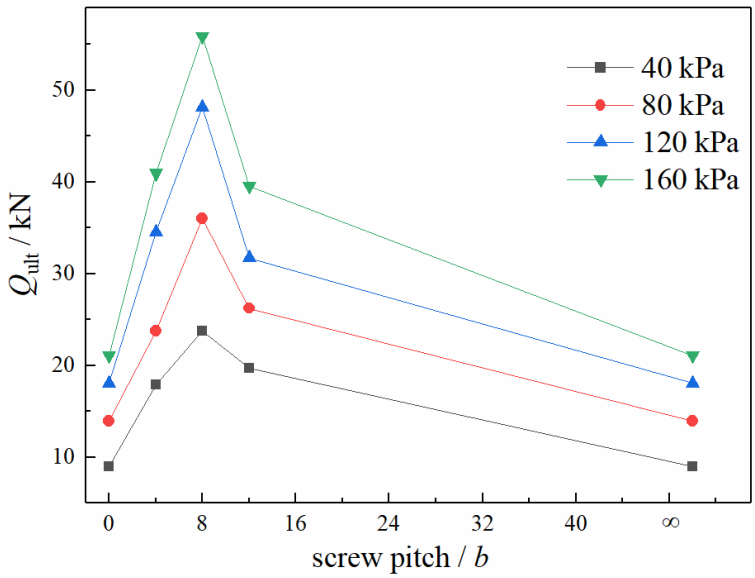

Figure 9. Variation curves of the ultimate bearing capacity of the screw shear plates.

Remarkably, Figure 9 confirms the existence of an optimal screw pitch for the screw pile. According to the test results, the optimal screw pitch was 8*b*. The bearing capacity weakened when the screw pitch was larger or smaller than the optimal screw pitch. This phenomenon is related to the two typical failure modes of screw piles: IBF and CSF. As mentioned, whether the screw pitch is greater than the critical screw pitch distinguishes the IBF mode from the CSF mode and is also closely related to the optimal screw pitch. Overall, both values are considered the same.

As shown in Figure 10a, when the screw pile is in the CSF mode, the screw pitch has almost no influence on the ultimate bearing capacity, and the lateral bearing capacity of the pile is mainly influenced by the physical parameters of the soil. The lateral bearing capacity is provided by the soil shear stress of the cylindrical surface, and its calculation is as follows:

$$Q_f = \int p_h \tan \varphi + c$$

Here, p_h, φ, and c are the lateral earth pressure, internal friction angle, and soil cohesion, respectively.

When the screw pitch exceeded a certain range, the failure mode changed to the IBF mode. The lateral resistance comprises the tip bearing capacity of the screw teeth and the skin friction of the shaft. In this case, the interaction between the screw teeth and the soil becomes more complex. Determining the final soil failure mode has become the major issue in calculating the bearing capacity of the screw pile. Several representative failure modes are shown in Figure 11 [25,27,31]. However, the failure mode closer to the practical condition is uncertain.

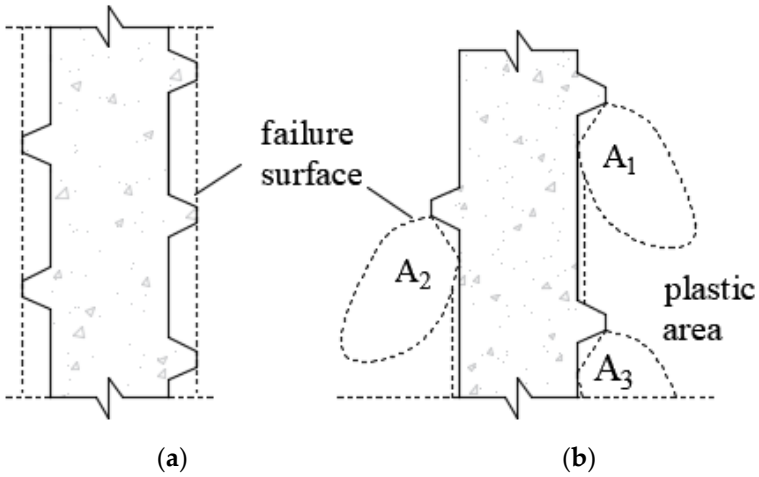

Figure 10. Failure modes of the screw pile. (**a**) CSF and (**b**) IBF.

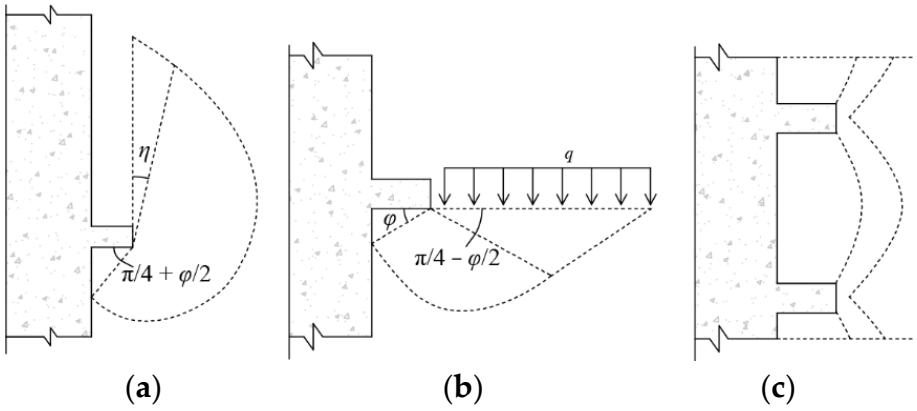

Figure 11. Theoretical assumptions of the failure mode under the screw teeth. (**a**) Meyerhof, (**b**) Terzaghi, and (**c**) arch.

Through the above-performed analysis, 8*b* was shown to be the optimal screw pitch in the test. Next, the variation of the soil stress and the soil deformation of the 8*b* screw shear plate are discussed to obtain the mechanical characteristics of the screw teeth and soil under the IBF state.

3.2. Mechanical Characteristics of Screw Teeth

3.2.1. Soil Stress

As shown in Figure 12, the distribution of the final soil stress under different overburden pressures was analyzed. The additional soil stress decreased with increased distance between the soil and screw teeth along the loading direction. The influence area of the stress transfer did not exceed 8*b*. The main influence area (yellow area) of the screw teeth was within 4–5*b* in the horizontal direction and 2–3*b* in the vertical direction. Meanwhile, the core influence area (red area) was within 2*b* and 1*b* in both these directions. The stress distribution diagram shows that when the screw pitch was 8*b*, the failure mode of the soil under the screw teeth was not the shear failure along the outer edge of the screw teeth but similar to the compression failure of the strip foundation. Therefore, 8*b* is greater than the critical screw pitch.

Meanwhile, the final soil stress distribution of the 12*b* screw shear plate ($s > s_{cr}$) was drawn under pressures of 40 kPa and 120 kPa (Figure 13). The distribution law of soil stress was shown to be similar to that of the 8*b* screw shear plate. In other words, when the screw pitch was larger than the critical pitch, the final distribution law of soil stress was similar, including the influence range of the screw teeth and the distribution form of soil stress.

In order to analyze the load transfer law of the screw teeth, the soil stress variations during the loading process were analyzed. Taking the 120 kPa monitoring data as an example, the results are shown in Figure 14.

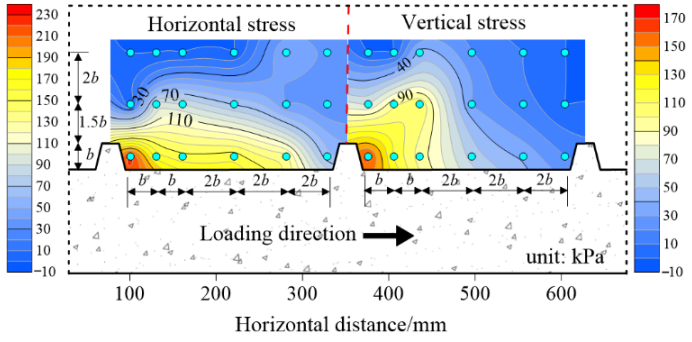

(**a**)

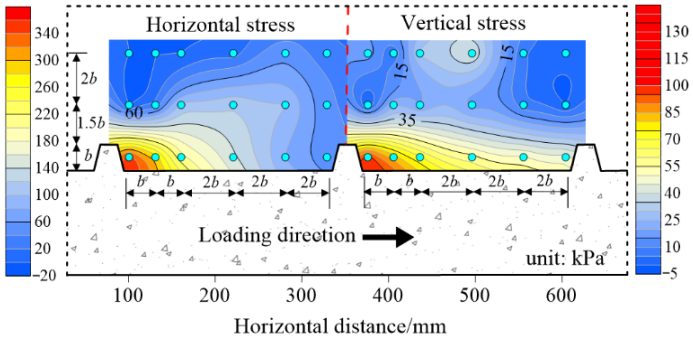

(**b**)

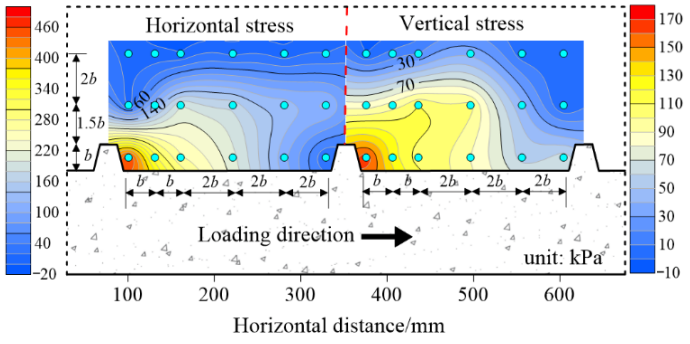

(**c**)

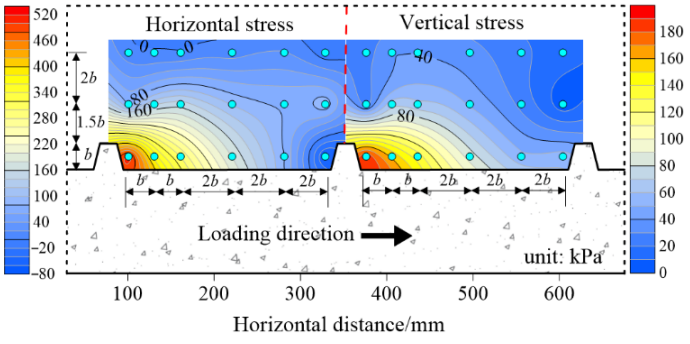

(**d**)

Figure 12. Final soil stress distribution of the 8*b* screw shear plate. (**a**) 40 kPa, (**b**) 80 kPa, (**c**) 120 kPa, and (**d**) 160 kPa.

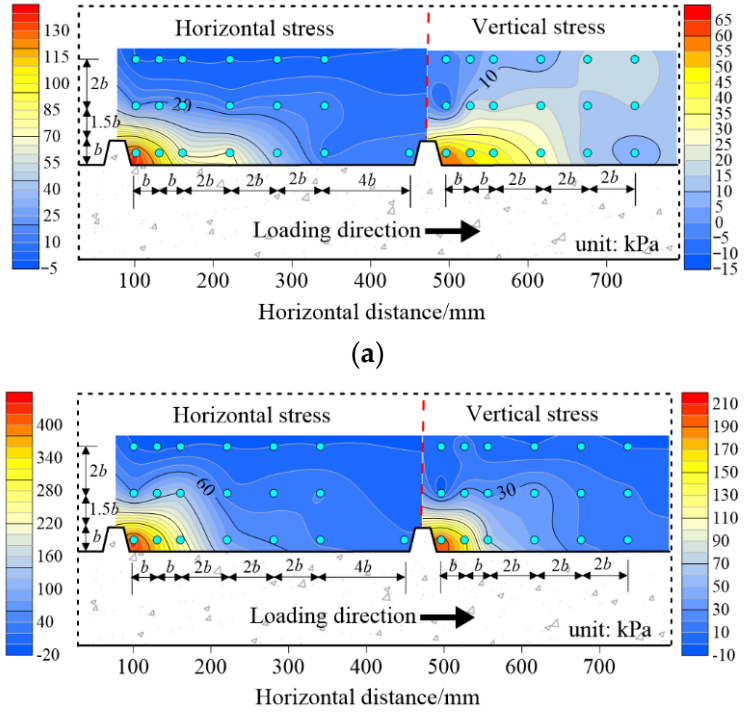

Figure 13. Final soil stress distribution of the 12*b* screw shear plate. (**a**) 40 kPa and (**b**) 120 kPa.

When the load *Q* was 6 kN, the stress level was relatively low. The variation range of soil stress in the horizontal and vertical directions was small. In this case, the soil deformation was still in an elastic state, and the stress change was mainly concentrated at the bottom of the screw teeth. Moreover, the soil stress variations on the left side of the middle screw tooth were shown to be negative. This is because the load transfer of the left screw tooth was small and did not influence the variations, while the middle screw tooth tended to move to the right, causing a decrease in the soil stress on its left side, hence the negative value. Similarly, the soil near the right screw tooth also showed a similar trend.

With an increase in load, the load transfer range was expanded when *Q* reached 18 kN, and the additional soil stress increased significantly. However, the soil stress on the left side of the middle screw teeth continued to decrease, indicating that the additional stress from the left screw tooth was not transmitted to this area. When *Q* reached 27 kN, the screw shear plate displacement was 12.26 mm. Subsequently, the soil produced certain plastic deformations, and the influence area of the screw teeth started to stabilize. When *Q* reached 48 kN, the screw shear plate reached its ultimate bearing state. The soil stress on the left side of the middle screw tooth also started increasing gradually. The influence area of the screw teeth was fixed, that is, 2–3*b* in the vertical direction and 4–5*b* in the horizontal direction, as mentioned above.

3.2.2. Soil Deformation

For the 8*b* screw shear plate, the final deformation of the soil around the screw teeth is shown in Figure 15, where the cyan line is the initial position of the deformation line and the red line is the final position.

The soil deformation was mainly concentrated in the range of 1–2*b* in the vertical direction, which is also the main influence area of the load transfer and gradually decreased in the horizontal direction. When exceeding the range of 4–5*b*, the soil deformation trend was similar to that of the circular pile. The additional force became relatively weak, and the soil deformation is mainly caused by the shear stress of the screw shear plate. Meanwhile, the degree of soil deformation showed that the severe deformation area was mainly in the

range of 2*b* in the horizontal direction and 1.5*b* in the vertical direction. This is consistent with the influence zone of soil stress.

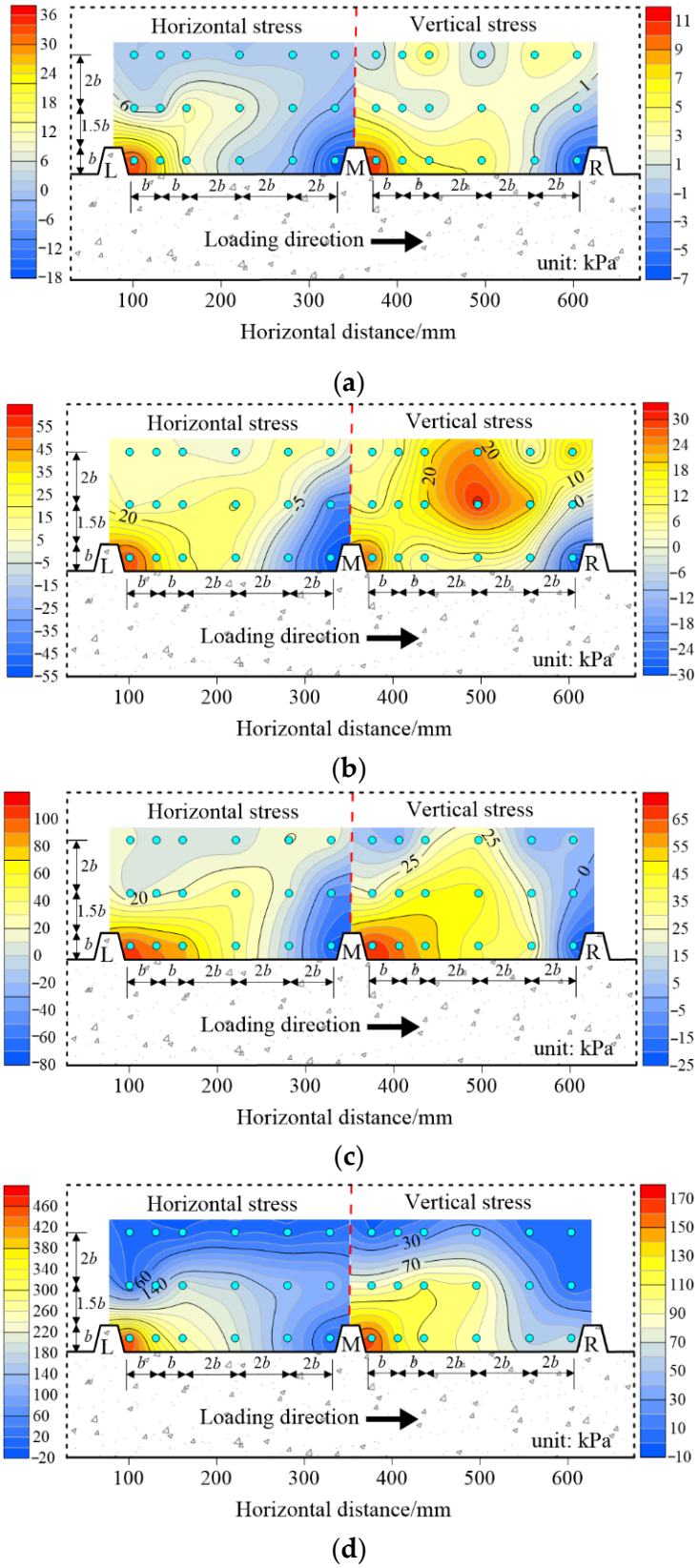

Figure 14. Variation of soil stress under different pressures. (**a**) Q = 6 kN, u = 0.21 mm, (**b**) Q = 18 kN, u = 2.14 mm, (**c**) Q = 27 kN, u = 12.26 mm, and (**d**) Q = 48 kN, u = 39.53 mm.

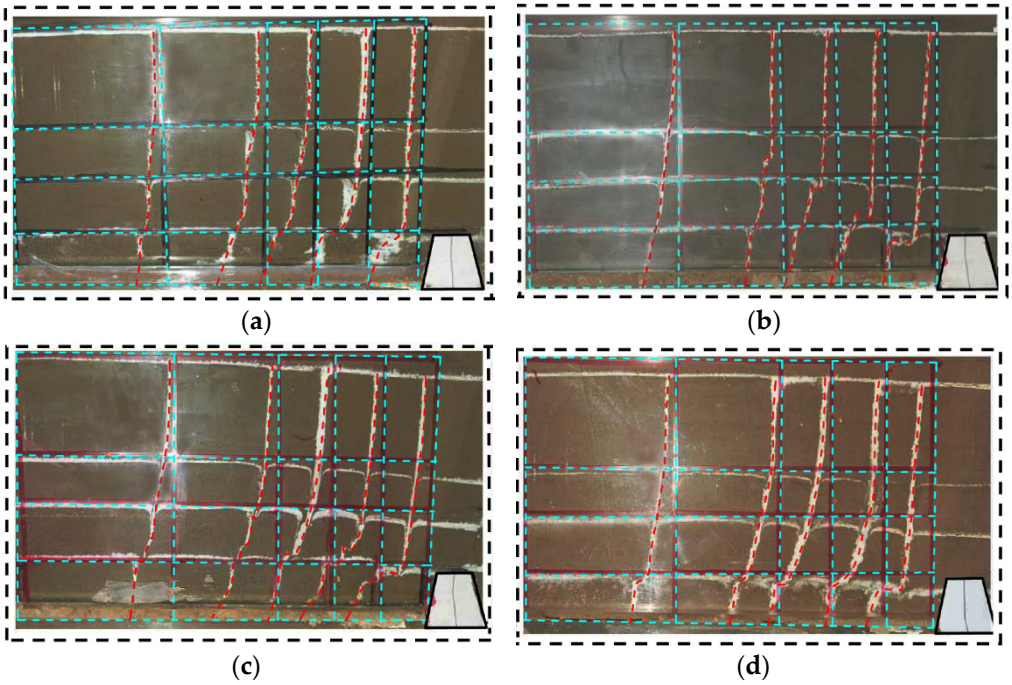

Figure 15. Final deformation of 8*b* screw shear plate. (**a**) 40 kPa, (**b**) 80 kPa, (**c**) 120 kPa, and (**d**) 160 kPa.

3.3. Theoretical Analysis

Based on the abovementioned test results, a theoretical failure model for screw teeth was established, and the relevant derivation was conducted.

Assuming that the forces on the OA surface of the screw tooth are uniformly distributed, the force distribution is shown in Figure 16. The resultant force of the normal stress σ and shear stress τ is p_t.

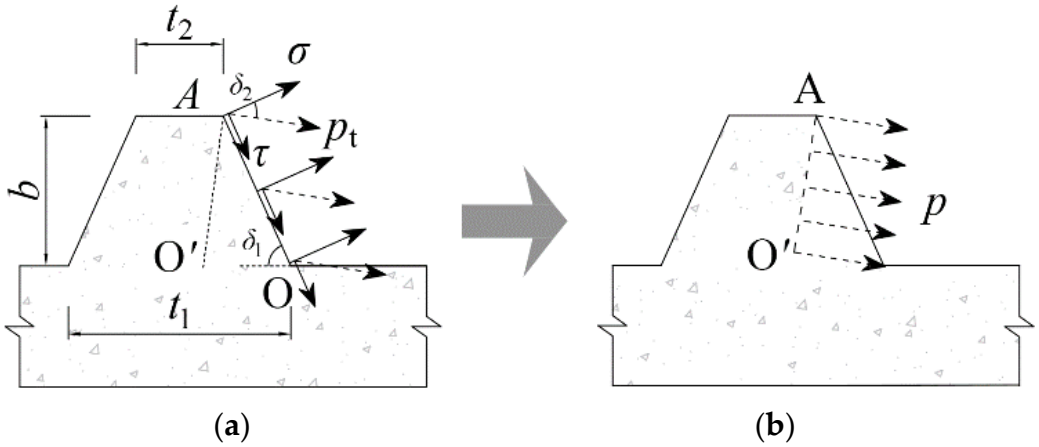

Figure 16. Forces on screw teeth. (**a**) Practical and (**b**) projection.

The shear stress on the screw teeth $\tau = \sigma\tan\delta_0 + c_0$ under ultimate load, where δ_0 and c_0 are the friction angle and cohesion between the pile–soil interface, respectively. The inclination angle of the screw teeth is δ_1, and the angle between p_t and normal stress is δ_2. The calculation method for δ_1 and δ_2 is as follows:

$$\tan\delta_1 = \frac{2b}{t_1 - t_2} \quad (1)$$

Here, b is the height of the screw teeth, and t_1 and t_2 are the bottom and top thicknesses of the screw teeth, respectively (Figure 16a).

$$\tan \delta_2 = \frac{\sigma \tan \delta_0 + c_0}{\sigma} = \tan \delta_0 + \frac{c_0}{\sigma} \tag{2}$$

The values of δ_0 and c_0 can be obtained from the relationship curve of Q_{ult}–p_0 of the plane shear plate (Figure 8). The fitting results show that $\delta_0 = 0.50\varphi$ and $c_0 = 0.57c$.

In order to illustrate the relationship between the applied force and failure surface, the force p_t on OA was projected on the virtual surface O′A, which is perpendicular to p_t. The corresponding pressure is p, as shown in Figure 16b. According to the geometrical relationship, the conversion relationship between p_t and p can be obtained as follows:

$$p = \frac{p_t}{\cos \delta_2} \tag{3}$$

According to the law of soil stress variation and deformation obtained from the test, the final failure pattern of the soil around the screw teeth is assumed, as shown in Figure 17. The main influence area of the screw teeth is divided into three parts. The OAE is the core passive earth pressure failure zone, BCD is the subsequent passive earth pressure failure extension zone, and the ABDE is the transition zone between both passive failure zones. Correspondingly, AE is the passive failure surface generated by the pressure of the OA surface, and BC is the passive failure surface generated by the pressure of the BD surface. According to the stress characteristics of the screw teeth and soil, the following simplifications and assumptions were made:

(1) It was assumed that the vertical pressure on the CD surface is uniformly distributed and that the vertical pressure on the DE surface increases uniformly from p_0 to p_E, where p_0 is the overlying soil pressure and p_E is the normal stress at point E.
(2) The friction force and cohesion on the CE surface were not considered.
(3) The plastic curved surface AB was simplified as a plane. The normal and shear stresses were assumed to increase linearly. The normal and shear stresses at points A and B were p_A and τ_A and p_0 and τ_0.

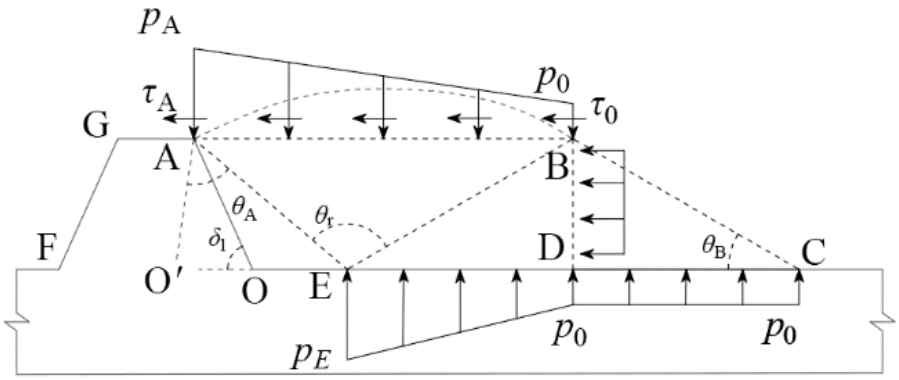

Figure 17. Final failure mode of the soil.

First, the maximum principal stress on the BD surface of the passive failure zone BCD could be easily obtained following the Mohr–Coulomb yield criterion:

$$p_1 = p_0 \tan \theta_A^2 + 2c \tan \theta_A \tag{4}$$

Second, the force analysis of the ABDE region was conducted, as shown in Figure 18.

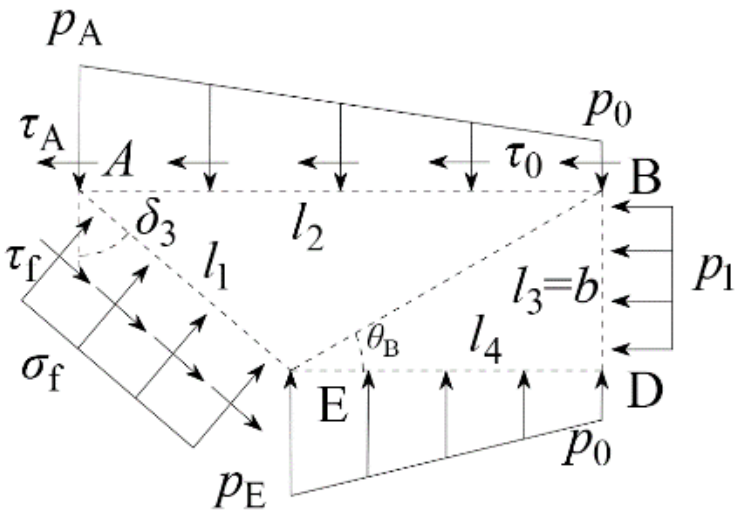

Figure 18. Force in the ABDE area.

Next, the normal stress σ_f and tangential stress τ_f on the AE surface were solved. According to the force balance in the vertical and horizontal directions, the following could be obtained:

Horizontal:

$$p_1 b + \frac{\tau_0 + \tau_A}{2} l_2 = (\sigma_f \cos\delta_3 + \tau_f \sin\delta_3) l_1 \tag{5}$$

Vertical:

$$\frac{p_0 + p_E}{2} l_4 + (\sigma_f \sin\delta_3 - \tau_f \cos\delta_3) l_1 - \frac{p_0 + p_A}{2} l_2 = 0 \tag{6}$$

Simultaneously, given that the sum of moments at point A is 0, the following could be obtained:

$$\frac{p_1 b^2}{2} + \frac{p_0 {l_2}^2}{2} + \frac{(p_A - p_0){l_2}^2}{6} = p_0 l_4 \left(\frac{l_4}{2} + l_1 \sin\delta_3\right) + \frac{(p_E - p_0) l_4}{2} \left(\frac{l_4}{3} + l_1 \sin\delta_3\right) + \frac{\sigma_f {l_1}^2}{2} \tag{7}$$

Here,

$$l_1 = \tfrac{b}{\cos\delta_3};\ l_2 = \lambda_1 b; l_3 = b; l_4 = \tfrac{b}{\tan\theta_B}; \lambda_1 = \tfrac{1}{\tan\theta_B} + \tan\delta_3;$$
$$\delta_3 = \tfrac{\pi}{2} + \theta_A - \delta_1 - \delta_2$$

Moreover,

$$\tau_f = \sigma_f \tan\varphi + c \tag{8}$$

Therefore, the following results could be obtained:

$$\sigma_f = \frac{\xi_2}{\xi_1} p_0 + \frac{\xi_3}{\xi_1} c \tag{9}$$

Here,

$$\xi_1 = \lambda_3(\tan\delta_3 - \tan\varphi) - \tfrac{1}{4\tan\theta_B \cos{\delta_3}^2} - \lambda_2(1 + \tan\varphi\tan\delta_3)$$
$$\xi_2 = \tfrac{\lambda_1\lambda_3\tan\theta_B - \lambda_3}{2\tan\theta_B} - \tfrac{\frac{\tan\theta_A^2}{2} + \frac{{\lambda_1}^2}{3} + \lambda_3 - \lambda_2}{2\tan\theta_B} - \lambda_2\left(\tan\theta_A^2 + \tfrac{\lambda_1\tan\varphi}{2}\right)$$
$$\xi_3 = \lambda_3 - \tfrac{\tan\theta_A}{2\tan\theta_B} - \lambda_2(2\tan\theta_A + \lambda_1 - \tan\delta_3)$$
$$\lambda_2 = \tfrac{1}{\tan\theta_B}\left(\tfrac{1}{2\tan\theta_B} + \tan\delta_3\right); \lambda_3 = \tfrac{1}{2\tan\theta_B} - \left(\tfrac{1}{3\tan\theta_B} + \tan\delta_3\right); \lambda_4 = \tfrac{\lambda_1\lambda_3 - \frac{{\lambda_1}^2}{6\tan\theta_B}}{\lambda_1\tan\varphi}$$

After calculating the normal and tangential stresses on the AE surface and projecting them in the horizontal direction, the bearing capacity on the screw teeth could be obtained. Subsequently, the bearing capacity provided by each screw tooth was calculated as follows:

$$Q_0 = (\sigma_f \cos\delta_3 + \tau_f \sin\delta_3) l_1 L_0 = \left[(1 + \tan\delta_3 \tan\varphi)\sigma_f \tan\delta_3 c\right] b L_0 \quad (10)$$

Here, L_0 is the length of the screw teeth on the screw shear plate.

The critical screw pitch can be determined following the failure mode; that is, the critical screw pitch is equal to the length of the OC. The calculation equation is as follows:

$$s_{cr} = l_1 \sin\delta_3 + 2l_4 - \frac{b}{\tan\delta_1} = \left(\tan\delta_3 + \frac{2}{\tan\theta_B} - \frac{1}{\tan\delta_1}\right) b \quad (11)$$

For the screw shear plate with a screw pitch larger than the critical screw pitch, its bearing capacity is mainly composed of two parts: the bearing capacity of the screw teeth' influential area and the friction area (Figure 19).

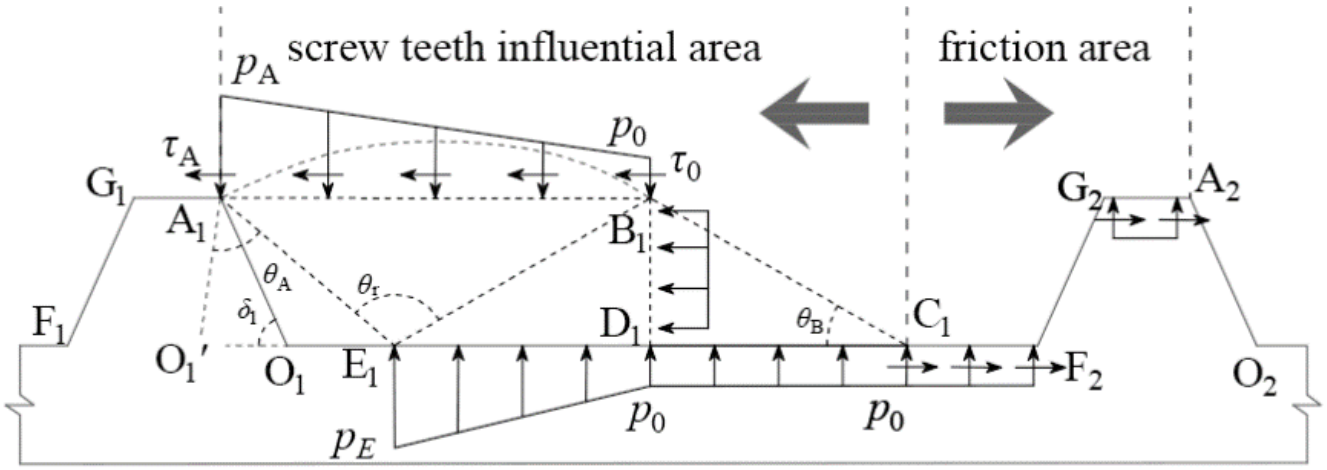

Figure 19. Force division of the screw teeth.

Therefore, the bearing capacity of the screw shear plate was calculated as follows:

$$\begin{aligned} Q_{ult} &= nQ_0 + (p_0 \tan\delta_0 + c_0) L_p L_0 \\ &= n[(1 + \tan\delta_3 \tan\varphi)\sigma_f \tan\delta_3 c] b L_0 + (\sigma \tan\delta_0 + c_0) L_p L_0 \end{aligned} \quad (12)$$

Here, n is the number of screw teeth, Lp is the total length of the friction area, and $L_p = L_B + nt_2 - ns_{cr}$

4. Discussion

When calculating the equivalent friction angle δ_2, the normal stress σ on the OA surface was assumed to be equal to the normal stress p_1 on the BD surface, which is inconsistent with the practical normal stress. Therefore, it needs to be amended. In this paper, the repeated iterations method is used to make the calculated value of δ_2 close to the accurate value. The calculated value was considered accurate if the error was less than a certain value.

First, the normal stress on the screw OA surface needs to be obtained. According to the geometrical relationship of the Mohr circle, the relationship between the stress on the failure surface AE and the normal stress p on the virtual surface O′A could be calculated (Figure 20).

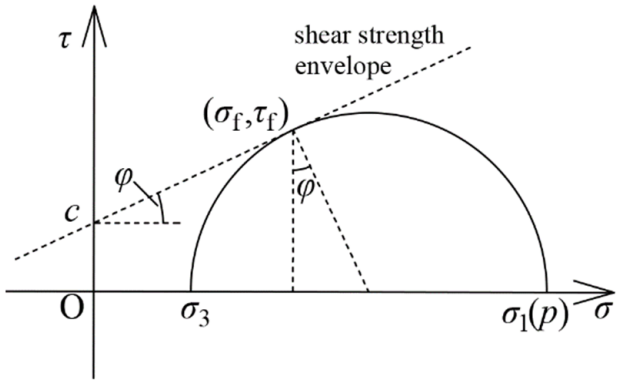

Figure 20. Mohr circle of soil stress.

As shown in Figure 20,

$$p = \sigma_f + \tau_f \tan\varphi + \tau_f / \cos\varphi = \sigma_f + \tau_f \frac{1+\sin\varphi}{\cos\varphi} \quad (13)$$

According to Equation (3), the resultant force p_t on OA can be obtained. Subsequently, the corresponding normal stress σ could be obtained through the following steps:

$$\sigma = p\cos\delta_2^2 \quad (14)$$

The approximate solution of the δ_2 could be obtained iteratively according to the following steps:

(1) Assuming $\sigma = p_1$, the initial value δ_{20} of the δ_2 could be calculated.
(2) Substituting the value into the equations in Section 3.3 and calculating the normal stress σ on the surface OA again.
(3) Substitute the new σ into Equation (2) to obtain the new value of δ_2, which is δ_{21}.
(4) Compare δ_{21} and δ_{20}; when $\frac{\delta_{21}-\delta_{20}}{\delta_{20}} \leq \Delta$, $\delta_2 = \delta_{21}$, where Δ is the criterion value, and it can be set at 0.1%.
(5) When $\frac{\delta_{21}-\delta_{20}}{\delta_{20}} > \Delta$, assign the value of the δ_{21} to δ_{20} and repeat Equations (2)–(4) until the criterion in Equation (4) is satisfied to obtain the calculated value of δ_2.

Taking the direct shear test of the 8*b* screw shear plate under 40 kPa as an example, the iterative process and results of the δ_2 are shown in Table 4. Obviously, the calculated value of the δ_2 is similar to the practical value after only three iterations.

Table 4. Calculation process of δ_2.

Iterations	p_0/kPa	tanδ_2	δ_{20}/°	σ/kPa	δ_{21}/°	Deviation/%	if < Δ	Final δ_2/°
1	40.0	0.32	17.676	353.84	16.121	8.80	NO	16.031
2		0.29	16.121	369.26	16.035	0.53	NO	
3		0.29	16.035	370.13	16.031	0.02	YES	

The plane shear plate is the basis of the theoretical calculation, without verification. According to Equation (11), the critical screw pitch s_{cr} under the test conditions was 4.7*b*. The screw pitch of the 4*b* screw shear plate was less than the critical screw pitch. Assuming that the failure surface forms a cladding surface along the outer edge of the screw teeth, the calculation formula for the ultimate bearing capacity is $Q_{ult} = A_T(p_0 \tan\varphi + c)$. The bearing capacity of the 8*b* and 12*b* screw shear plates was calculated using Equation (10). Next, the theoretical formula was verified through the test results of the screw shear plates with different screw pitches (Table 5).

Table 5. Comparison between the theoretical and measured values.

s	p_0	40 kPa	80 kPa	120 kPa	160 kPa
4b	Q_t/kN	19.28	27.76	36.24	44.72
	Q_{ult}/kN	17.86	23.72	34.55	40.95
	η/%	7.95	17.03	4.89	9.21
8b	Q_t/kN	21.26	32.33	43.40	54.48
	Q_{ult}/kN	23.78	36.00	48.15	55.88
	η/%	−10.60	−10.19	−9.87	−2.51
12b	Q_t/kN	16.90	25.43	33.97	42.51
	Q_{ult}/kN	19.69	26.22	31.71	39.54
	η/%	−14.17	−3.01	7.13	7.51

Q_t and Q_{ult} are the theoretical and measured values of the ultimate bearing capacity of the screw shear plates, respectively. η is the deviation rate, which was calculated using the following formula:

$$\eta = \frac{Q_t - Q_{ult}}{Q_{ult}} \times 100\% \quad (15)$$

The theoretical values of the ultimate bearing capacity of the screw shear plates were similar to the measured values for all conditions. The maximum deviation between the theoretical and measured values was 17.03% but within 10% overall, which proves the accuracy of the theoretical calculation method proposed in this paper.

5. Conclusions

Through large-scale direct shear tests of the screw shear plates, the contact relationship between the screw teeth and soil was studied. The law of stress variation and deformation of the soil around the screw teeth was analyzed. A theoretical failure model was established, and the calculation equations for the critical screw pitch (s_{cr}) and the bearing capacity were proposed and verified. The following are the major conclusions:

(1) The bearing capacity of the screw shear plate was larger than that of the plane shear plate, indicating that the bearing capacity can be significantly improved by the screw pile compared with the circular pile.

(2) With an increase in the screw pitch, the bearing capacity of the screw shear plate first increased and then decreased. There was an optimal screw pitch, enabling the bearing capacity and the bearing effect of the soil around the screw teeth to reach their maximum. The optimal screw pitch made the screw reach the IBF state, which is the critical screw pitch.

(3) For the screw piles in the IBF state, the main influence range of the screw teeth was about 4–5b along the loading direction and 1–2b along the vertical direction. The corresponding values of the core influence zone were about 1–2b and 1b.

(4) The rationality of the proposed method for calculating the bearing capacity of the screw shear plate and the critical screw pitch in the IBF state was verified by the test results. The calculation equation of s_{cr} contains the shear strength parameters of the soil and the geometric parameters of the screw teeth, which have better applicability as s_{cr} than a general fixed value.

In this paper, the screw pile was developed into the screw shear plate to study its bearing characteristics, which can be more convenient for obtaining the law of deformation and stress variation of the soil around the screw teeth. Moreover, useful research results were obtained. However, due to its limited length, this paper only discussed the bearing characteristics of the screw pile under the loess condition. For the other type of soil, its bearing characteristics may vary. Meanwhile, the punching shear failure of the screw teeth was not considered. The abovementioned problems can be further discussed in a follow-up study to improve the theoretical system of the screw pile.

Author Contributions: Conceptualization, J.M. and L.L.; methodology, J.M. and L.L.; investigation, T.M. and H.G.; resources, T.M. and Y.T.; data curation, J.M.; writing—original draft preparation, J.M.; writing—review and editing, J.M. and T.M.; supervision, L.L.; project administration, J.M.; funding acquisition, L.L. All authors have read and agreed to the published version of the manuscript.

Funding: This work was supported by the National Natural Science Foundation of China (42077248 and 41877285), and the Fundamental Research Funds for the Central Universities of China (300102289201 and 300102281102).

Data Availability Statement: Not applicable.

Conflicts of Interest: The authors declare no conflict of interest.

References

1. Peng, Y.; Liu, J.; Ding, X.; Jiang, C. Performance of X-section concrete pile group in coral sand under vertical loading. *China Ocean Eng.* **2020**, *34*, 621–630. [CrossRef]
2. Ren, L.W.; Guo, W.D.; Yang, Q.W. Analysis on bearing performance of Y-shaped piles under compressive and tensile loading. *Proc. Inst. Civ. Eng.-Geotech. Eng.* **2020**, *173*, 58–69. [CrossRef]
3. Zhang, M.; Xu, P.; Cui, W.; Gao, Y. Bearing behavior and failure mechanism of squeezed branch piles. *J. Rock Mech. Geotech. Eng.* **2018**, *10*, 935–946. [CrossRef]
4. Ma, H.W.; Liu, L.; Wang, P.; Yuan, S.; He, Q.R.; Yang, X.L. Calculation method and mechanism of ultimate side resistance of screw pile. *Mar. Georesour. Geotech.* **2021**. [CrossRef]
5. Karalar, M.; Dicleli, M. Effect of thermal induced flexural strain cycles on the low cycle fatigue performance of integral bridge steel H-piles. *Eng. Struct.* **2016**, *124*, 388–404. [CrossRef]
6. Li, W.; Stuedlein, A.W.; Chen, Y.; Liu, H.; Cheng, Z. Response of pile groups with X and circular cross-sections subject to lateral spreading: 3D numerical simulations. *Soil Dyn. Earthq. Eng.* **2019**, *126*, 105774. [CrossRef]
7. Sakr, M. Performance of helical piles in oil sand. *Can. Geotech. J.* **2009**, *46*, 1046–1061. [CrossRef]
8. Spagnoli, G. Some considerations regarding the use of helical piles as foundation for offshore structures. *Soil Mech. Found. Eng.* **2013**, *50*, 102–110. [CrossRef]
9. Mohajerani, A.; Bosnjak, D.; Bromwich, D. Analysis and design methods of screw piles: A review. *Soils Found.* **2016**, *56*, 115–128. [CrossRef]
10. Zheng, X.; Chen, X.; Zhang, J. Stress analysis of screw-bored compaction cast-in-place piles. *IOP Conf. Ser. Earth Environ. Sci.* **2021**, *719*, 032003. [CrossRef]
11. Malik, A.A.; Kuwano, J.; Tachibana, S.; Maejima, T. Effect of helix bending deflection on load settlement behavior of screw pile. *Acta Geotech.* **2019**, *14*, 1527–1543. [CrossRef]
12. Perko, H.A. *Helical Piles: A Practical Guide to Design and Installation*, 1st ed.; John Wiley & Sons Inc.: Hoboken, NJ, USA, 2009.
13. Kurian, N.P.; Shah, S.J. Studies on the behaviour of screw piles by the finite element method. *Can. Geotech. J.* **2009**, *46*, 627–638. [CrossRef]
14. Meng, Z.; Chen, J.J.; Zhang, L.Y.; Wang, J.H. Field tests to investigate the installation effects of drilled displacement piles with screw-shaped shaft in clay. *J. Geotech. Geoenviron. Eng.* **2015**, *141*, 06015010. [CrossRef]
15. Chen, Y.D.; Deng, A.; Wang, A.T.; Sun, H.S. Performance of screw–shaft pile in sand: Model test and DEM simulation. *Comput. Geotech.* **2018**, *104*, 118–130. [CrossRef]
16. Aydin, M.; Bradka, T.; Kort, D. Osterberg cell load testing on helical piles. *Geo-Front.* **2011**, *2011*, 66–74. [CrossRef]
17. Livneh, B.; Naggar, M.H.M. Axial testing and numerical modelling of square shaft helical piles under compressive and tensile loading. *Can. Geotech. J.* **2008**, *45*, 1142–1155. [CrossRef]
18. Hawkins, K.; Thorsten, R. Load test results-large diameter helical pipe piles. *Contemp. Top. Deep. Found.* **2009**, 488–495. [CrossRef]
19. Tappenden, K.; Sego, D.; Robertson, P. Load transfer behaviour of full-scale instrumented screw anchors. *Contemp. Top. Deep Found.* **2009**, 472–479. [CrossRef]
20. Adams, J.I.; Klym, T.W. A study of anchorages for transmission tower foundations. *Can. Geotech. J.* **1972**, *9*, 89–104. [CrossRef]
21. Narasimha Rao, S.; Prasad, Y.V.S.N.; Veeresh, C. Behaviour of embedded model screw anchors in soft clays. *Geotechnique* **1993**, *43*, 605–614. [CrossRef]
22. Nasr, M.H. Performance-based design for helical piles. *Contemp. Top. Deep Found.* **2009**, 496–503. [CrossRef]
23. Meyerhof, G.G. The ultimate bearing capacity of foundations. *Geotechnique* **1951**, *2*, 301–332. [CrossRef]
24. Terzaghi, K.; Peck, R.B. *Soil Mechanics in Engineering Practice*, 3rd ed.; John Wiley & Sons Inc.: Hoboken, NJ, USA, 1967.
25. Shao, K.; Su, Q.; Liu, J.; Xiong, Z.; Wang, T. Optimization of inter-helix spacing for helical piles in sand. *J. Rock Mech. Geotech. Eng.* **2022**, *14*, 936–952. [CrossRef]
26. MOHURD (Ministry of Housing and Urban-Rural Development, PRC). *Technical Specification for Screw Concrete Pile*; MOHURD: Beijing, China, 2016. (In Chinese)
27. Qian, J.G.; Chen, H.W.; Jia, P.; Huang, M.S.; Hu, Y.Y. Experimental study of mechanical behaviours of grouting-screw pile interface. *Chin. J. Rock Mech. Eng.* **2013**, *32*, 1744–1749. (In Chinese)

28. MOHURD (Ministry of Housing and Urban-Rural Development, PRC). *Technical Code for Testing of Building Foundation Piles*; MOHURD: Beijing, China, 2014. (In Chinese)
29. Fateh, A.M.A.; Eslami, A.; Fahimifar, A. A study of the axial load behaviour of helical piles in sand by frustum confining vessel. *Int. J. Phys. Model. Geotech.* **2018**, *18*, 175–190. [CrossRef]
30. Ho, H.M.; Malik, A.A.; Kuwano, J.; Brasile, S.; Tran, T.V.; Mazhar, M.A. Experimental and numerical study on pressure distribution under screw and straight pile in dense sand. *Int. J. Geomech.* **2022**, *22*, 04022139. [CrossRef]
31. Ma, J.; Luo, L.; Ren, X.; Shi, H.; Yin, Y. Calculation method of bearing capacity of full concrete screw pile based on unified strength theory. *J. Shanghai Jiaotong Univ.* **2022**, *56*, 754–763. [CrossRef]